

Article

Identification of Dual-Target Inhibitors for Epidermal Growth Factor Receptor and AKT: Virtual Screening Based on Structure and Molecular Dynamics Study

Hanyu Yang ^{1,†}, Zhiwei Zhang ^{1,†} , Qian Liu ², Jie Yu ¹, Chongjin Liu ¹ and Wencai Lu ^{1,*}

¹ College of Physics, Qingdao University, Qingdao 266071, China; 2020025451@qdu.edu.cn (H.Y.); 2020025442@qdu.edu.cn (Z.Z.); 2019020188@qdu.edu.cn (J.Y.); 2020020330@qdu.edu.cn (C.L.)

² School of Medicine and Pharmacy, Ocean University of China, Qingdao 266003, China; lq6360@stu.ouc.edu.cn

* Correspondence: wencailu@qdu.edu.cn

† These authors contributed equally to this work.

Abstract: Epidermal growth factor EGFR is an important target for non-small cell lung (NSCL) cancer, and inhibitors of the AKT protein have been used in many cancer treatments, including those for NSCL cancer. Therefore, searching small molecular inhibitors which can target both EGFR and AKT may help cancer treatment. In this study, we applied a ligand-based pharmacophore model, molecular docking, and MD simulation methods to search for potential inhibitors of EGFR and then studied dual-target inhibitors of EGFR and AKT by screening the immune-oncology Chinese medicine (TCMIO) database and the human endogenous database (HMDB). It was found that TCMIO89212, TCMIO90156, and TCMIO98874 had large binding free energies with EGFR and AKT, and HMDB0012243 also has the ability to bind to EGFR and AKT. These results may provide valuable information for further experimental study.

Keywords: small molecule inhibitors; EGFR; AKT; TCMIO; HMDB



Citation: Yang, H.; Zhang, Z.; Liu, Q.; Yu, J.; Liu, C.; Lu, W. Identification of Dual-Target Inhibitors for Epidermal Growth Factor Receptor and AKT: Virtual Screening Based on Structure and Molecular Dynamics Study. *Molecules* **2023**, *28*, 7607. <https://doi.org/10.3390/molecules28227607>

Academic Editors: Francisco Torrens and Alessandro Pedretti

Received: 15 September 2023

Revised: 3 November 2023

Accepted: 6 November 2023

Published: 15 November 2023



Copyright: © 2023 by the authors. Licensee MDPI, Basel, Switzerland. This article is an open access article distributed under the terms and conditions of the Creative Commons Attribution (CC BY) license (<https://creativecommons.org/licenses/by/4.0/>).

1. Introduction

The epidermal growth factor receptor (EGFR) is a transmembrane glycoprotein with an extracellular EGF binding domain and an intracellular tyrosine kinase domain. It plays a crucial role in regulating signaling pathways and controlling cellular proliferation. EGFR has been found to be overexpressed in many cancer cells [1]. This overexpression leads to autophosphorylation of its tyrosine residues, triggering a cascade of events that further affect cell proliferation, differentiation, and apoptosis [2]. EGFR overexpression has been observed in several types of cancer, including non-small cell lung cancer, pancreatic cancer, glial cell carcinoma, and other tissues. The inhibition of EGFR overexpression is considered a crucial strategy in current anti-cancer research [1]. Current studies on EGFR inhibitors can be divided into two main categories: monoclonal antibodies (mAb) and small molecule tyrosine kinase inhibitors (TKIs) [3]. EGFR inhibitors have emerged as a crucial class of antitumor drugs. The discovery of highly effective EGFR inhibitors is of paramount importance in the treatment of tumors, including lung cancer, cervical cancer, and breast cancer [4,5]. At present, a large number of small molecule TKIs targeting EGFR have been developed [6–10].

Gefitinib (IC₅₀ = 23–79 nM) and Erlotinib (IC₅₀ = 80 nM) have been clinically used as first-generation representative EGFR-TKIs compared to standard chemotherapy [11]. These drugs act as reversible competitive inhibitors of ATP to prevent EGFR autophosphorylation [12]. In the treatment of breast cancer, Afatinib (IC₅₀ = 0.5 nM), a second-generation EGFR-TKI, has gained significant popularity [13–15]. In addition, a third-generation TKI called Osimertinib (IC₅₀ = 12 nM) specifically targets EGFR-T790M resistance mutations that occur due to the use of first-generation TKIs [16,17].

In the field of natural product inhibitors of EGFR, research has shown that sesquiterpene lactones, chalcone, and phenolic compounds can be synergistically combined with small molecule inhibitors to enhance drug sensitivity and improve therapeutic outcomes [18]. Abou-Zied HA et al. developed a novel xanthine derivative that incorporates the chalcone component for investigating potential EGFR inhibitors and successfully obtained compound **11**, which exhibited an IC₅₀ value of 0.3 μ M against the target enzyme [19]. Abdelgawad et al. developed innovative phenolic compounds as potential inhibitors of EGFR and COX-2. Their research resulted in the identification of compounds C4 and G4, which demonstrated impressive inhibitory activity with IC₅₀ values of 0.9 and 0.5 μ M, respectively [20]. Furthermore, an interesting study conducted by N Nerdy et al. revealed that sesquiterpene lactones derived from veronica amygdaline defile exhibited potential anticarcinogenic effects through the inhibition of EGFR expression [21].

However, despite the potent activity demonstrated by these EGFR inhibitors, challenges such as drug resistance and weak efficacy in cells and in vivo settings persist [22]. Therefore, there is an urgent necessity for the development of novel EGFR inhibitors. This urgency arises from the fact that the activation of EGFR profoundly impacts a multitude of signaling mechanisms within cells. As the downstream protein of EGFR, AKT assumes a crucial role in regulating cell proliferation and survival. Moreover, AKT acts as a constitutively active kinase that promotes the survival of NSCLC cells [23]. Notably, the heightened activity of AKT has been associated with the persistence of drug resistance against first-generation EGFR TKIs [24,25].

The computational study of drugs plays an important role in the field of drug discovery and has gained widespread usage in identifying potential new drug candidates. The strategy of screening large virtual molecular libraries uses a series of methodologies, including molecular docking, the construction of pharmacodynamic groups, and the application of quantitative structure–activity relationships (QSARs). These approaches have been effectively employed in the quest for identifying inhibitors targeting EGFR or AKT [26–28]. Currently, there is an increasing emphasis on the research of protein inhibitors that target dual or even multiple targets. Alessia Bono et al. conducted a study on a novel dual-target inhibitor for SARS-CoV-2 MPRO, resulting in the identification of six potential compounds [29]. Similarly, Edgar et al. utilized the MD method to investigate dual inhibitors for G9a and DNMT1, successfully identifying compounds exhibiting dual activity [30]. However, there have been very few computational studies for dual-target inhibitors of EGFR and AKT. Tarozzi A et al. undertook the design and investigation of several quinazoline derivatives to study EGFR and AKT dual inhibitors [31]. In this study, our objective was to search for dual inhibitors targeting EGFR and AKT in the traditional Chinese medicine on immune-oncology (TCMIO) and human endogenous library (HMDB) databases [32,33] using a pharmacophore model, molecular docking, and molecular dynamics (MD) simulation methods. The identified inhibitor candidates can potentially contribute valuable insights for further experimental investigations on novel inhibitors targeting EGFR and AKT.

2. Results and Discussion

2.1. Results of Pharmacophore and Molecular Docking Screening

A set of 20 inhibitor compounds, each possessing distinct active structures, was employed to construct pharmacophore models. Finally, a pharmacophore model with two aromatic rings, two hydrophobicity characteristics, and one H-bond donor characteristic (Figure 1) was selected based on the overlap and accuracy values.

Using the developed pharmacophore model, a comprehensive screening process was carried out on a total of 240,956 compounds from the TCMIO and HMDB datasets. 3252 compounds successfully passed the screening criteria, and, subsequently, the top 20% of compounds (456 in TCMIO and 194 in HMDB) were selected based on ranking the RMSD (root mean square deviation) scores.

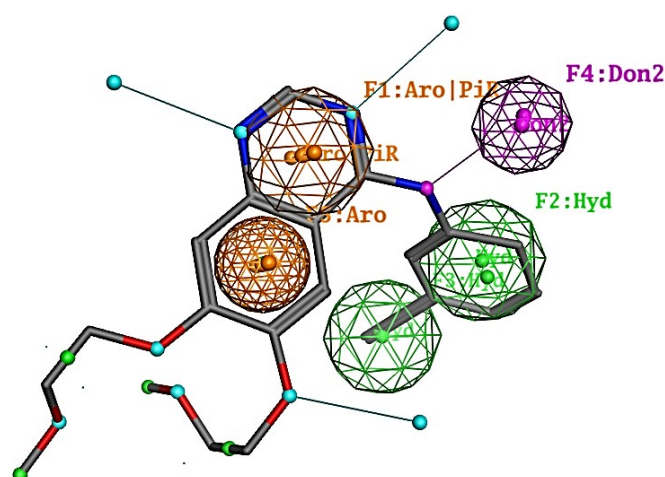


Figure 1. Pharmacophore with the F1-F5 features constructed from 20 EGFR positive compounds and its overlap with Erlotinib. Green: Hydrophobic centroid. Purple: H-bond donor. Orange: Aromatic center.

In order to ascertain the accuracy and reliability of molecular docking, the receiver operating characteristic (ROC) curve for the validation index was calculated based on the true positive rate and false positive rate. The resulting area under the curve (AUC) value was determined to be 0.707 (Figure 2). Furthermore, the docking result of protein inhibitors showed that the RMSD value of Erlotinib was 1.35 Å, and its docking score of the best conformation was -7.44 kcal/mol. Similarly, the AKT ligand, A-443654, demonstrated an RMSD of 1.43 Å, with a corresponding docking score of -8.42 kcal/mol. The ROC validation results and the docking results of the inhibitors from EGFR and AKT demonstrated the reliability of the molecular docking method. Based on the analysis of docking results, it was observed that the selected compounds were capable of effectively binding to the ligand-binding sites of EGFR and AKT. Finally, a total of seven compounds with the best docking scores were chosen for further analyses (Figure 3). Met769 is the key residue of EGFR inhibitors (such as Erlotinib), contributing to protein structure stabilization or functional regulation. It interacts with the hinge region of 4-aniline quinazoline scaffold through specific binding interactions [34]. Table 1 shows that the compounds TCMIO89212, TCMIO90156, TCMIO98874, HMDB0014570, and HMDB0037450 formed H-bond interactions with the key residue Met769 of EGFR. Some of these compounds also formed hydrogen bonds with the residues Asp831, Gln767, Asn818, Thr830, and Lys721 (Table 1). A previous study by Yang et al. reported that the key residue Asp831 is involved in H-bond interactions [35]. It was suggested that strong interactions between compounds and Asp831 played an important role in inhibiting EGFR activity [36]. The docking results shown in Table 1 indicated that TCMIO5312, TCMIO98874, HMDB0012243, and HMDB0037450 formed H-bond interactions with Asp831. As depicted in Figure 4, the compounds were successfully docked in the binding pocket of EGFR.

The docking scores of TCMIO98874, TCMIO90156, and TCMIO89212 with EGFR were -7.96 , -7.51 , and -7.06 kcal/mol, respectively. Figure 4 shows the 3D docking structures with EGFR for all compounds compared to Erlotinib. The 2D interactions of TCMIO98874, TCMIO90156, TCMIO89212, and Erlotinib docking to the EGFR ligand-binding site are shown in Figure 5, in which Erlotinib formed H-bond interactions with Met769, Leu768, and Gln767. On the other hand, TCMIO89212, TCMIO98874, and TCMIO90156 also formed H-bond interactions with Met769. Interestingly, in addition to its interactions with Met769, TCMIO98874 also formed H-bond interactions with Asp831.

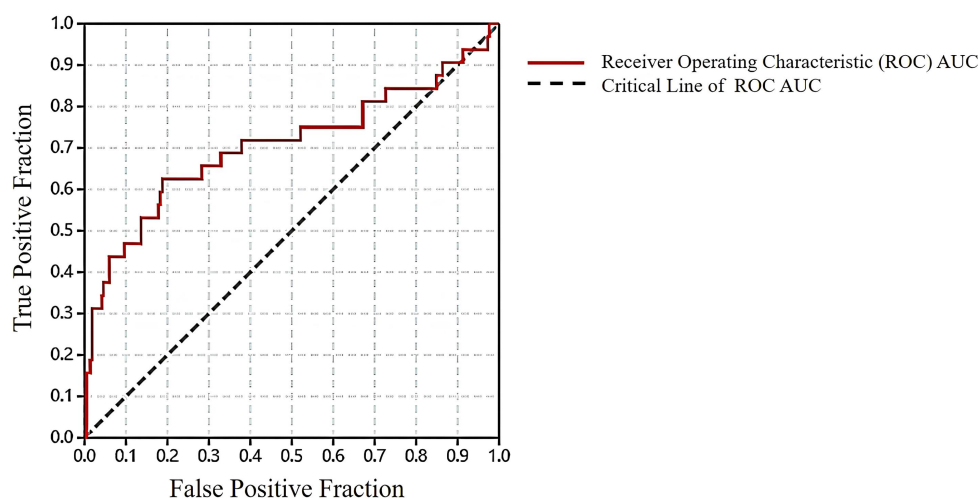


Figure 2. ROC verification of molecular docking method.

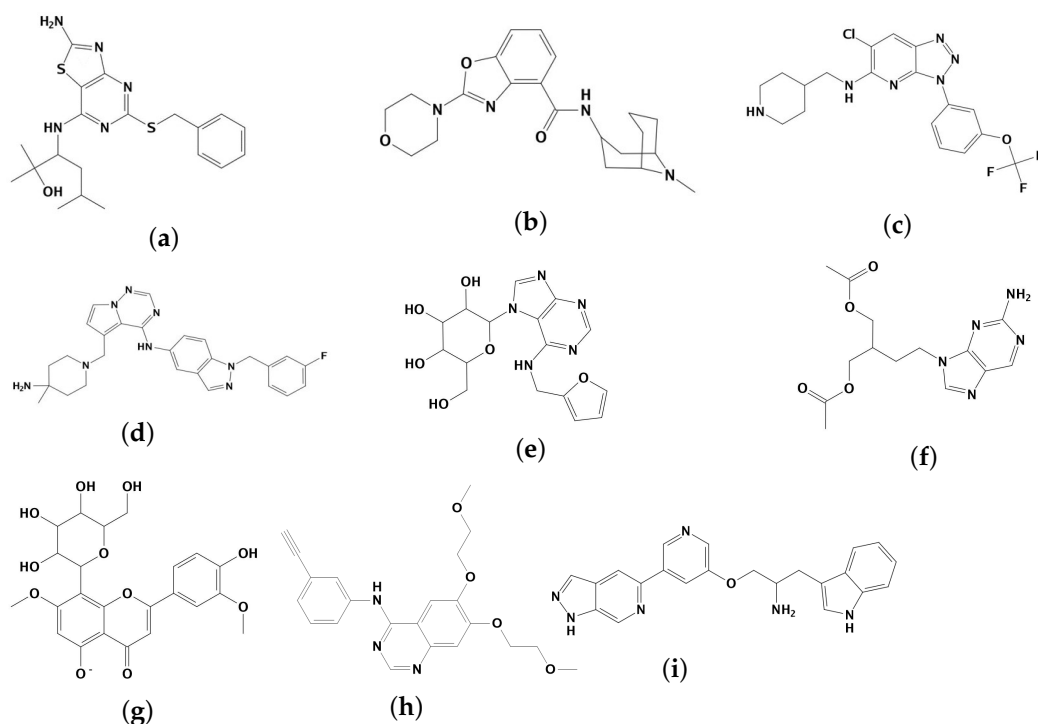
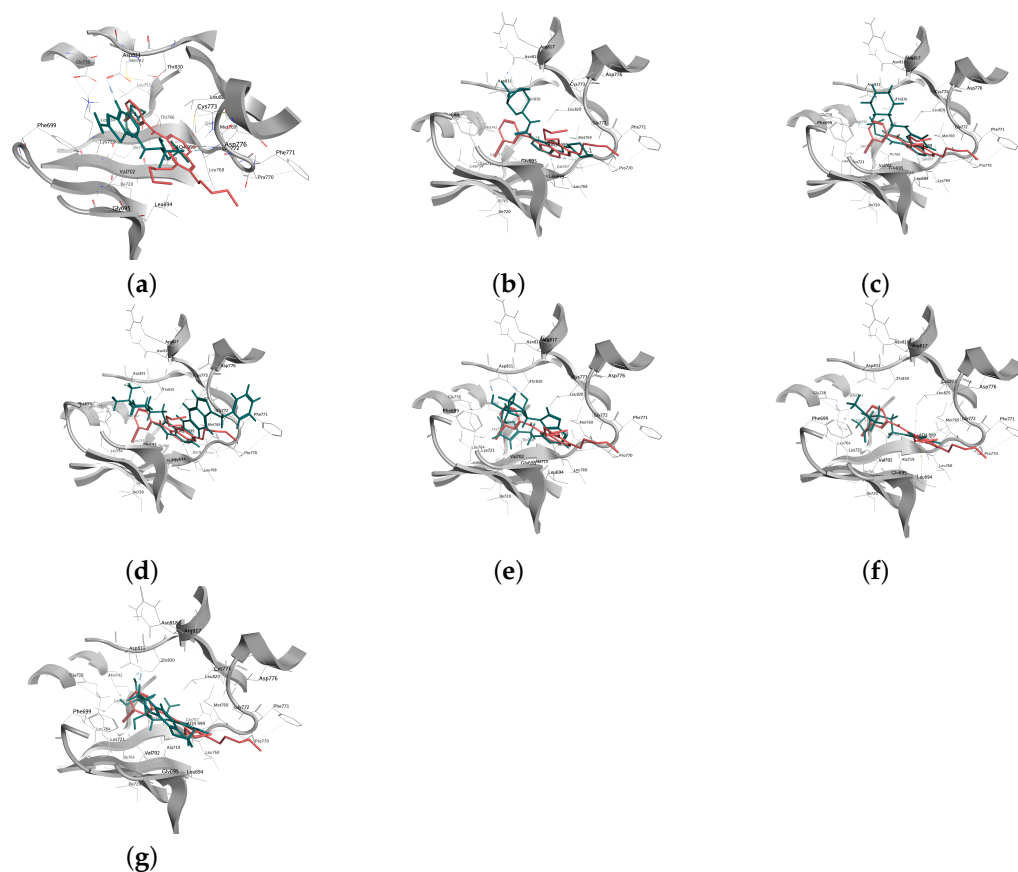


Figure 3. Two-dimensional structures of (a) TCMIO5312, (b) TCMIO89212, (c) TCMIO90156, (d) TCMIO98874, (e) HMDB0012243, (f) HMDB0014570, (g) HMDB0037450, (h) Erlotinib, and (i) A-443654.

In addition, according to the docking results of the seven compounds with AKT (Table 2), TCMIO90156, TCMIO89212, and TCMIO98874 exhibited docking scores of -8.28 , -8.24 , and -8.00 kcal/mol, respectively. The docking score of inhibitor A-443654 was calculated to be -8.42 kcal/mol. As indicated in Table 2, A-443654 demonstrated H-bond interactions with Glu230, Asn280, Asp290, Ala232, and Lys181 at the AKT binding site. Additionally, it exhibited an electrostatic interaction with Asp293. On the other hand, TCMIO89212 formed H-bond interactions with Met229, Met282, and Ala332 (Figure 6). TCMIO90156 primarily interacted with Glu236 at the AKT binding site, while TCMIO98874 predominantly interacted with Asp440. TCMIO90156 exhibited a predominant interaction with Glu236 in AKT, while TCMIO98874 primarily interacted with Asp440 in AKT.

Table 1. GBVI/WSA dG docking scores of the EGFR–ligand complexes.

Compound ID	Docking Score (kcal/mol)	Interaction Type	Key Amino Acid	Ligand Efficiency (kcal/mol)
TCMIO5312	−7.72	H-donor H-acceptor	Glu831, Met742, Asp831 Asp831	−0.276
TCMIO89212	−7.06	H-acceptor	Met769, Gln767	−0.252
TCMIO90156	−7.51	H-acceptor H-acceptor	Met769, Lys721, Gln767 Met769	−0.256
TCMIO98874	−7.96	H-donor H-acceptor	Asp831 Met769, Gln767	−0.221
HMDB0012243	−7.29	H-donor	Asp831	−0.270
HMDB0014570	−7.33	H-acceptor	Met769	−0.318
HMDB0037450	−7.85	H-donor H-acceptor Ionic	Asp776, Gln767 Met769, Thr830, Asp831, Lys721 Lys721	−0.231
Erlotinib	−7.37	H-acceptor	Met769	−0.254

**Figure 4.** Three-dimensional docking structures with EGFR of the candidate inhibitors (green) (a) TCMIO5312, (b) TCMIO89212, (c) TCMIO90156, (d) TCMIO98874, (e) HMDB0012243, (f) HMDB0014570, (g) HMDB0037450, and Erlotinib (red).

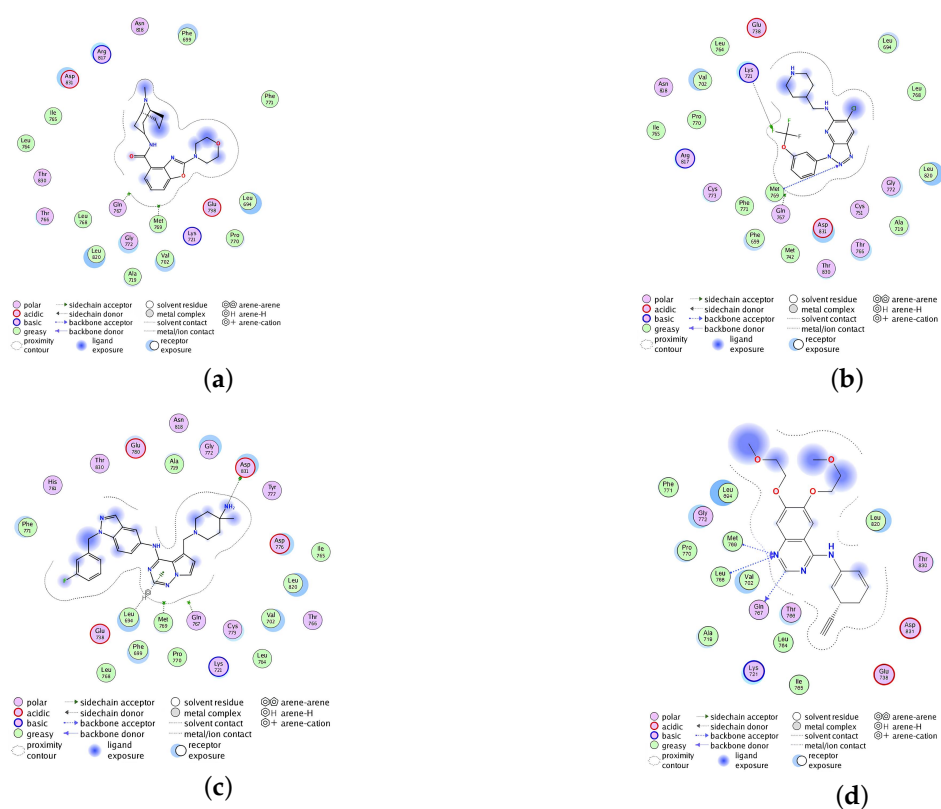


Figure 5. Schematic 2D representations of the interactions between EGFR and (a) TCMIO89212, (b) TCMIO90156, (c) TCMIO98874, and (d) Erlotinib, respectively.

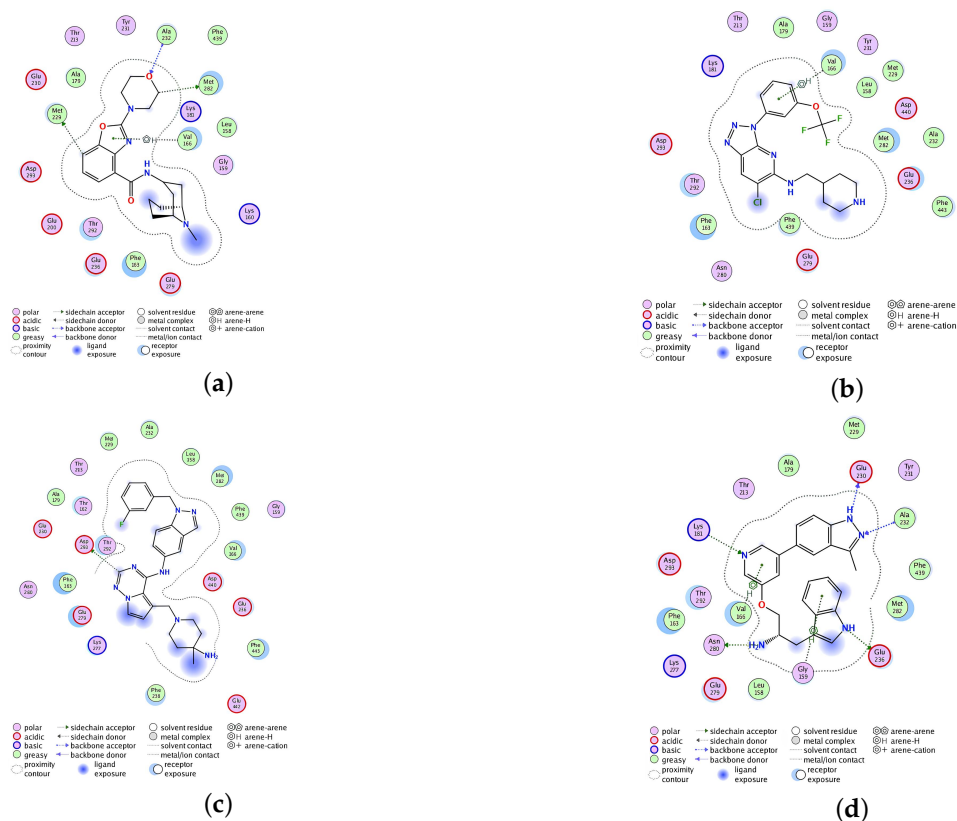


Figure 6. Schematic 2D representations of the interactions between AKT and (a) TCMIO89212, (b) TCMIO90156, (c) TCMIO98874, and (d) A-443654, respectively.

Table 2. GBVI/WSA dG docking scores of the AKT–ligand complexes.

Compound ID	Docking Score (kcal/mol)	Interaction Type	Key Amino Acid	Ligand Efficiency (kcal/mol)
TCMIO5312	−8.08	H-donor Ionic	Asn820, Glu236 Glu279	−0.289
TCMIO89212	−8.24	H-donor H-acceptor	Met229, Met282 Ala232	−0.294
TCMIO90156	−8.28	H-donor H-donor	Glu236 Asp831	−0.285
TCMIO98874	−8.00	H-donor Ionic	Asp440 Asp440	−0.222
HMDB0012243	−8.17	H-donor H-acceptor	Met229 Ala232, Asp293, Lys181	
HMDB0014570	−8.15	H-donor H-acceptor	Glu230 Asp293, Ala232	−0.354
HMDB0037450	−9.32	H-donor H-acceptor Ionic	Glu230, Gln236 Lys181, Glu236, Asp440 Lys181	−0.274
A-443654	−8.42	H-donor H-acceptor Ionic	Glu230, Asn280, Asp290, Glu236 Ala232, Lys181 Asp293	−0.280

2.2. MD Simulation Results

Using Amber22, we performed MD simulations on the complexes of seven compounds (TCMIO5312, TCMIO89212, TCMIO 90156, TCMIO98874, HMDB0012243, HMDB-0014570, and HMDB0037450) and the inhibitors of Erlotinib and A-443654 with EGFR and AKT. The analysis focused on the root mean square deviation (RMSD), root mean square fluctuation (RMSF), rotation radius (Rg), and hydrogen bonds formed during the simulation [37].

During the MD simulations, the ligands were initially placed at the binding site of the target protein based on molecular docking. Taking TCMIO90156 as an example, the 100 ns MD simulations were analyzed to observe the conformation changes of the ligand and target protein. Figure S1 showed that the composite structure of the protein with TCMIO90156 was gradually compacted during 100 ns. The protein structure underwent a gradual tightening process within the initial <20 ns timeframe. After a 20 ns MD run, the amplitude of protein structural changes appeared to be relatively small. Furthermore, the conformational changes occurring at the ligand–protein binding site did not exhibit noticeable variations during the 90 to 100 ns MD simulations, and TCMIO90156 became stabilized within the binding pocket.

2.2.1. RMSD, RMSF, and Rg Analyses

RMSD values obtained during MD simulations serve as indicators of conformational changes in receptor–ligand complexes [38]. As shown in Figure 7, it is apparent that the RMSD values of all the EGFR–compound complexes increased rapidly at the beginning of the MD simulations. Subsequently, the RMSD value for each complex in Figure 7 exhibited fluctuations within the range of 0.50 to 2.50 nm, suggesting the stability of these complexes. Notably, TCMIO90156, which possessed the most favorable binding free energy, achieved stabilization after 75 ns of simulation.

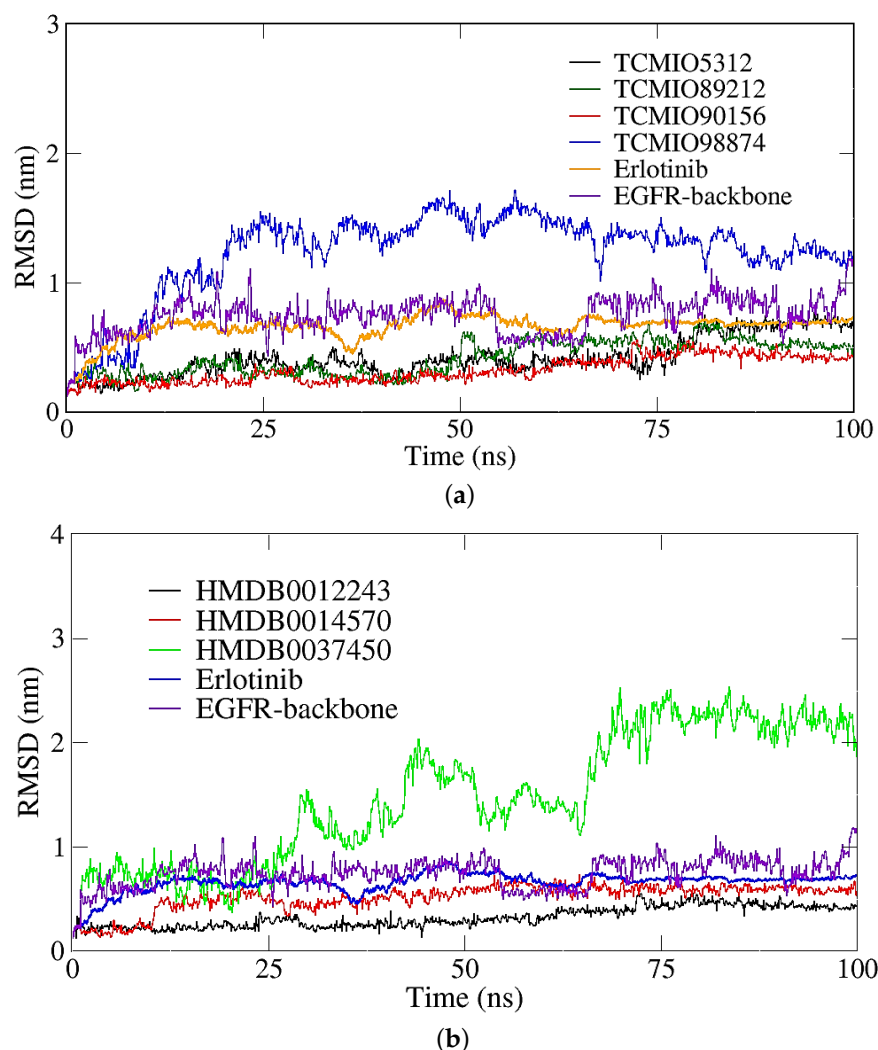


Figure 7. Backbone RMSD of the complexes of EGFR and inhibitor candidates screened from (a) TCMIO and (b) HMDB databases.

Figure 8 shows the RMSD results of the complex structures of seven compounds with AKT. In comparison to the control A-443654, the RMSD values for TCMIO90156, TCMIO5312, and HMDB0037450 demonstrated significant fluctuations, while the remaining compounds exhibited minimal fluctuations and were stabilized below 0.50 nm. During the 100 ns MD, the RMSD of TCMIO90156 experienced a rapid increase to 1 nm at 30 ns. However, the RMSD of TCMIO5312 gradually stabilized after 75 ns. As for HMDB0037450, its RMSD increased between 68 and 70 ns, reaching 0.7 nm, then decreased to 0.6 nm and remained stable. These observations suggest that all seven complexes of AKT remained stable throughout the MD simulations.

The RMSF values serve as indicators of the flexibility of complex structures. A higher RMSF value indicates greater flexibility [39]. In general, the terminus regions of protein structures exhibited higher flexibility as depicted in Figure 9. The majority of residues demonstrated similar RMSF values within the EGFR complex structures, suggesting that the binding of the compound to EGFR did not noticeably affect the stability of the protein structure.

It can be seen from Figure S2 that the RMSF values of the compounds bound to AKT were comparable to those of the EGFR complexes. Most residues exhibited RMSF values below 0.5 nm. Among the seven compounds, the average fluctuations of all compounds, except for TCMIO89212 and TCMIO90156, were lower than those of the control A-443654.

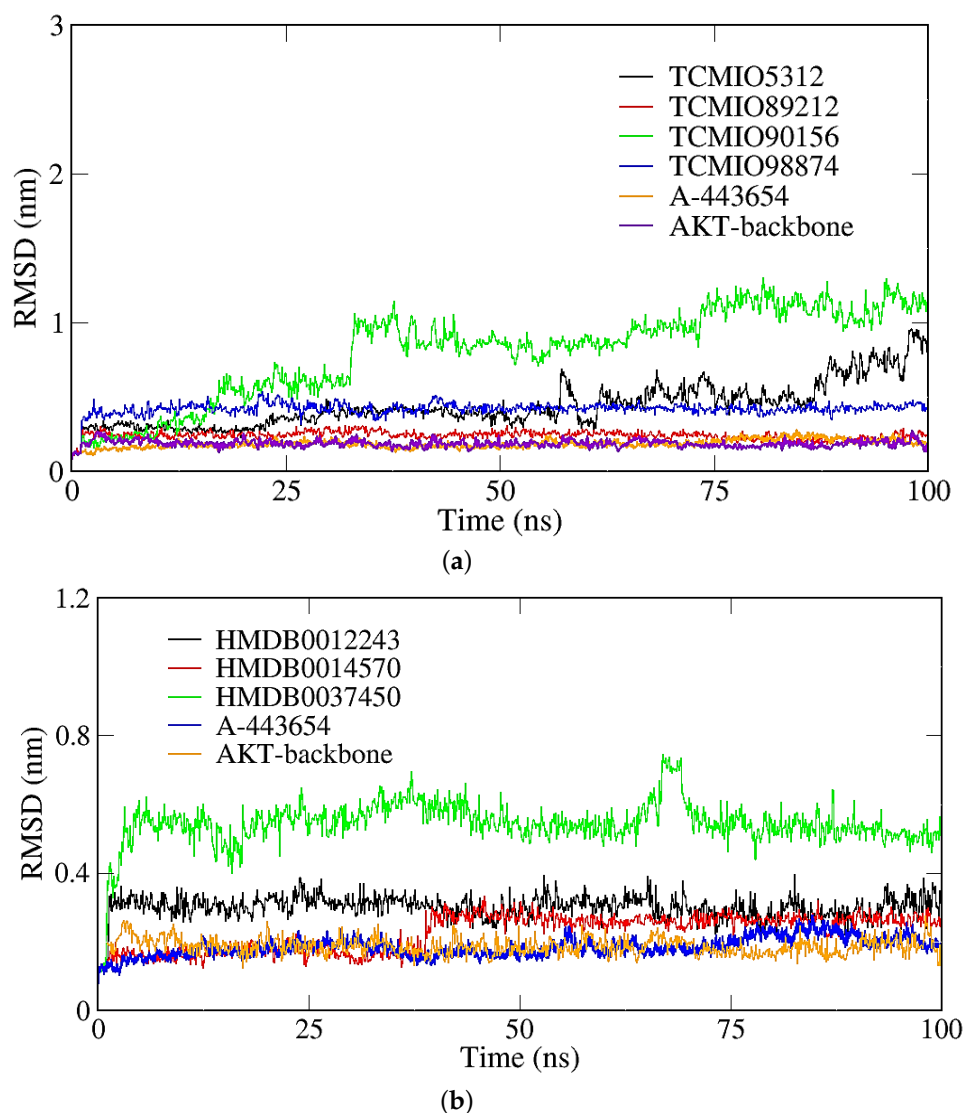
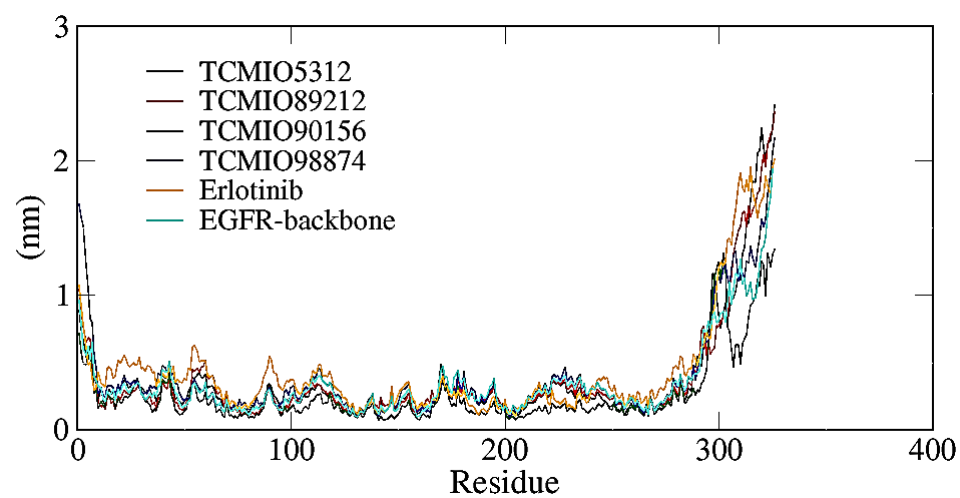


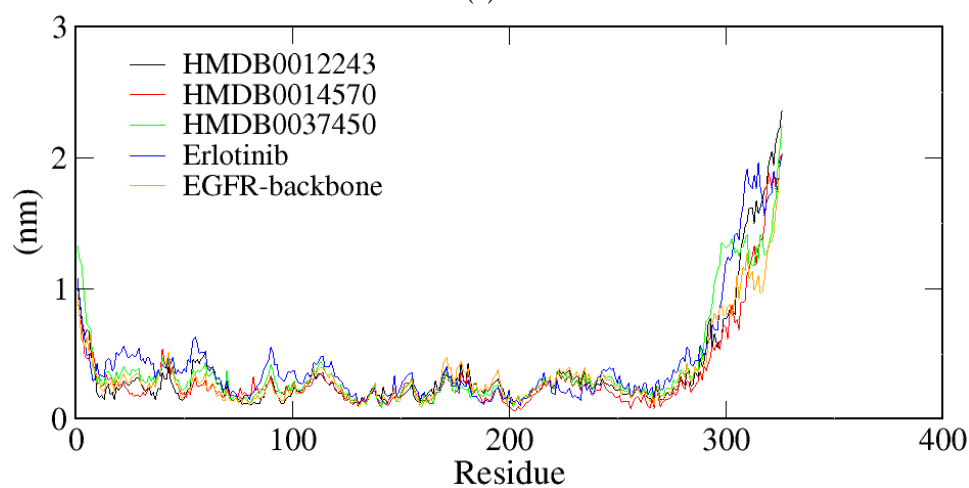
Figure 8. Backbone RMSD of the complexes of AKT and inhibitor candidates screened from (a) TCMIO and (b) HMDB databases.

The radii of Gyration (R_g) values were employed to assess the folding rate and the sizes of protein–compound complexes. R_g serves as a critical measure of protein compactness, with higher R_g values indicating lower protein compactness [39]. During the MD simulations, the R_g values were assessed. As depicted in Figure 10, it is evident that the R_g values fluctuated due to the inherent dynamism of the complexes. However, all the R_g values remained within the range of 2.0–2.80 nm, suggesting the absence of significant conformational changes. The complexes formed with TCMIO90156, TCMIO89212, TCMIO98874, TCMIO5312, HMDB0012243, and HMDB0037450 were observed to exhibit tighter structures compared with the Erlotinib complex. This observation suggests that these six compounds had a lesser impact on the tightness of the protein [40].

The AKT complexes analyzed in Figure S3 displayed R_g values ranging from 1.9 to 2.5 nm, suggesting the absence of noteworthy replaced conformational changes. Notably, all the compounds, except for TCMIO89212 and TCMIO90156, exhibited fluctuations around the 2 nm mark.

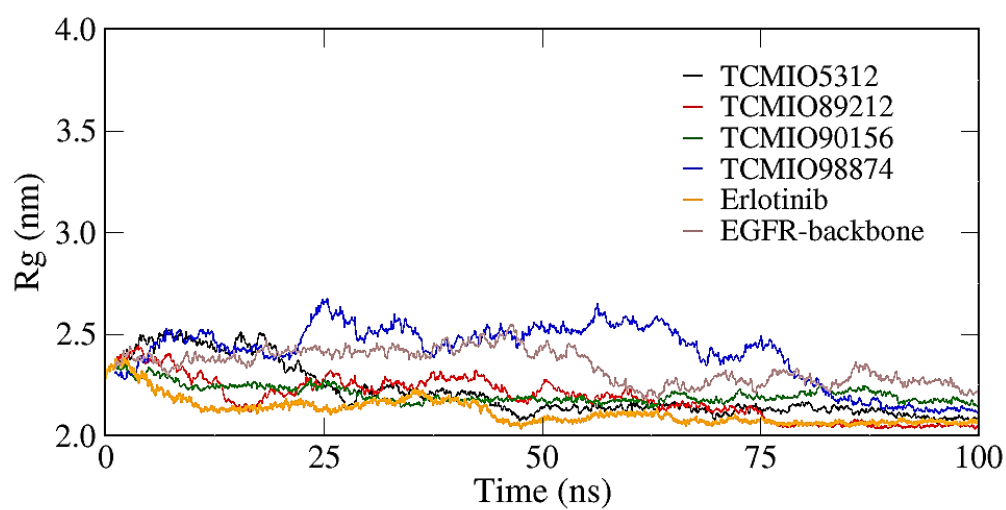


(a)



(b)

Figure 9. RMSF of the complex structures of EGFR with the TCMIO (a) and HMDB (b) compounds.



(a)

Figure 10. Cont.

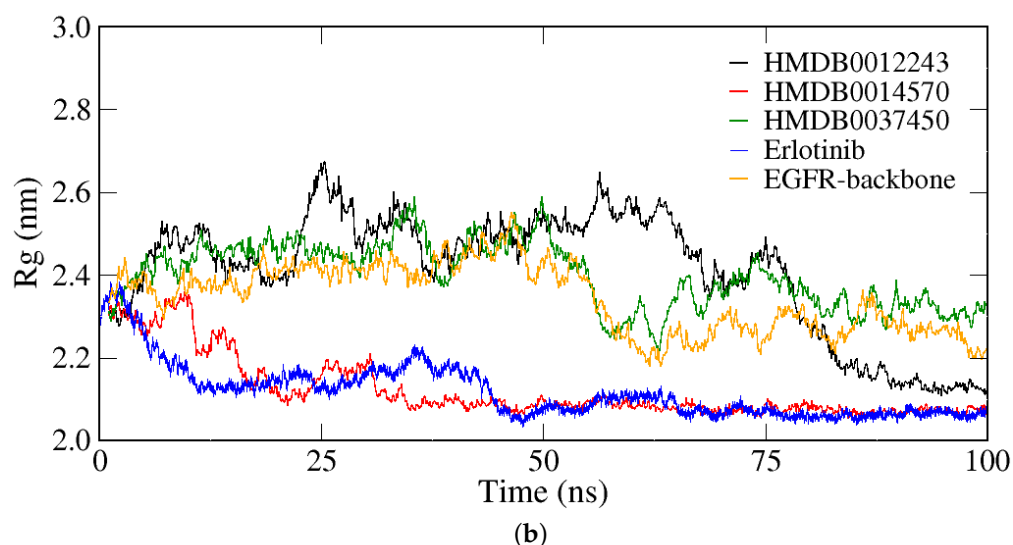


Figure 10. Radii of gyration (R_g) of the complex structures of EGFR with the TCMIO (a) and HMDB (b) compounds.

2.2.2. Analyses of H-Bonds

The H-bond module was utilized to determine the number of H-bonds formed between the ligand and receptor throughout the course of the MD simulations [41]. In general, it is expected that a ligand can establish at least two H-bonds with the receptor protein. Upon analyzing the H-bond count for three compounds in relation to EGFR, it is observed that the reference compound (Erlotinib) formed a maximum of four H-bonds during the 100 ns simulations. However, TCMIO98874, TCMIO5312, TCMIO90156, and TCMIO89212 were able to form a maximum of six, five, four, and three H-bonds with EGFR, respectively (Figure 11). As H-bond interactions are crucial in intermolecular binding, it was anticipated that TCMIO98874, TCMIO5312, and TCMIO90156 would exhibit efficient binding with EGFR [42].

Figure S4 showed that TCMIO98874, TCMIO90156, and TCMIO89212 have the potential to form a maximum of eight, six, and three H-bonds, respectively, with AKT. In comparison, the control compound A-443654 formed five hydrogen bonds.

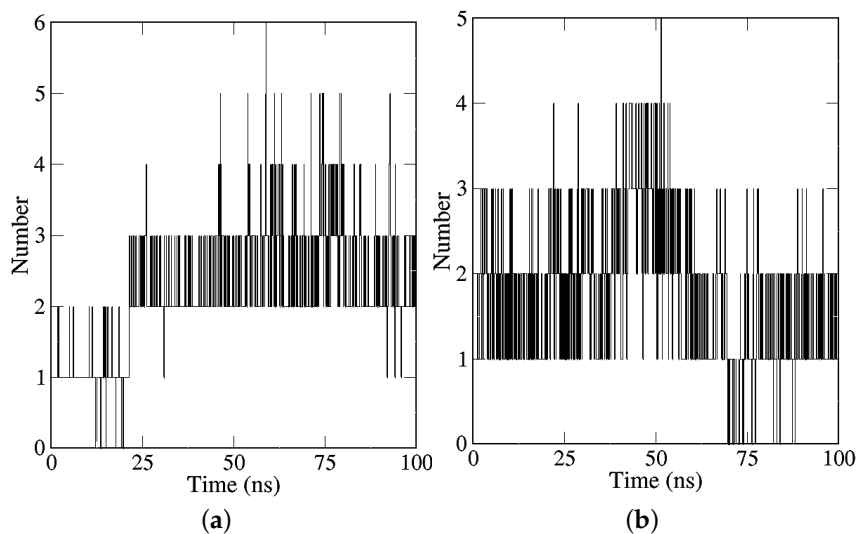


Figure 11. Cont.

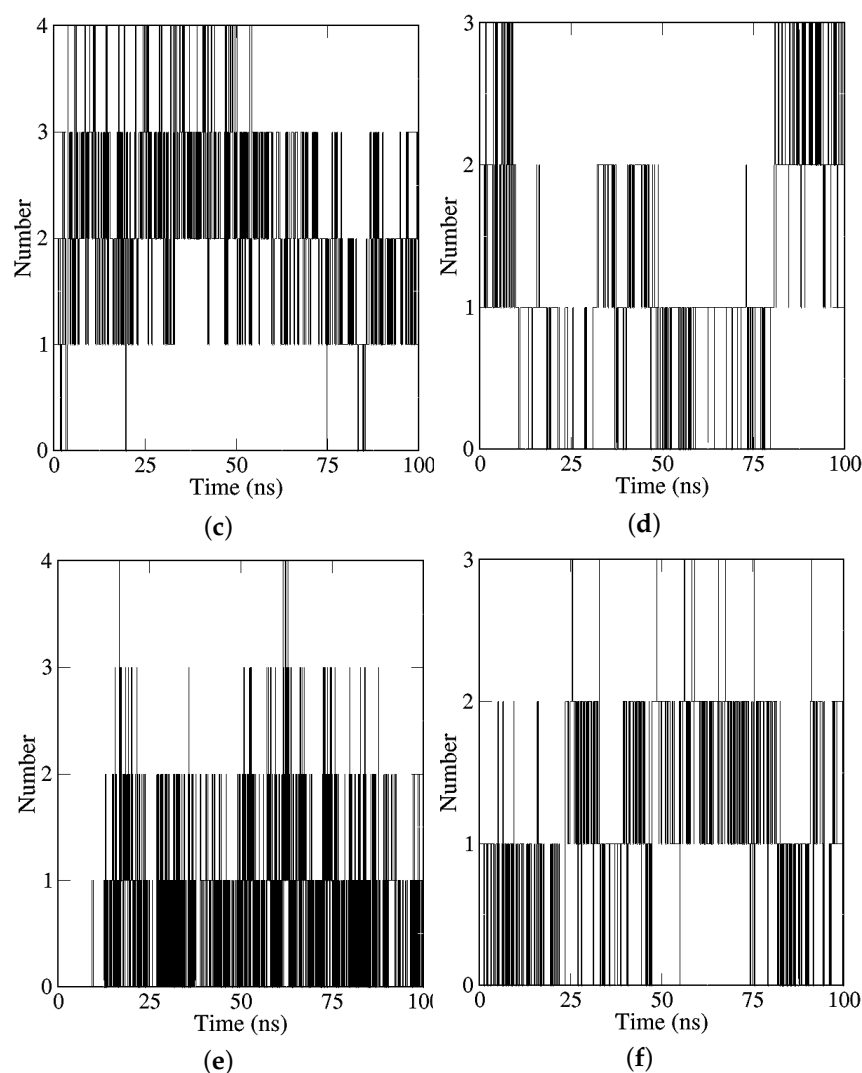


Figure 11. Numbers of intermolecular hydrogen bonds of (a) TCMIO98874, (b) TCMIO5312, (c) TCMIO90156, (d) TCMIO89212, (e) Erlotinib, and (f) EGFR-backbone binding to EGFR from 100 ns MD simulations.

2.2.3. Binding Free Energy Analyses

The MM-PBSA binding free energies were calculated using `gmx_MMPBA` [43]. The energy components, including van der Waals, electrostatic, polar solvation, and solvent accessible surface area (SASA) and total binding free energy, for the seven compounds are provided in Table 3.

Table 3. MM-PBSA binding free energies and energy components (kcal/mol) of the complexes of EGFR and screened TCMIO and HMDB compounds.

Ligands	$\Delta E_{\text{vander Waal}}$	$\Delta E_{\text{electrostatic}}$	$\Delta E_{\text{polar Solvation}}$	SASA	$\Delta G_{\text{binding}}$
TCMIO90156	−47.01	−131.48	147.32	−4.57	−35.74
TCMIO98874	−29.94	−243.41	247.05	−3.36	−29.66
TCMIO5312	−36.35	−146.94	160.09	−4.45	−27.65
TCMIO89212	−42.79	−149.06	169.92	−4.27	−26.20
HMDB0012243	−36.89	−49.90	70.77	−4.12	−20.14
HMDB0014570	−40.65	−16.51	45.41	−3.92	−15.67
HMDB0037450	−15.32	−49.39	54.12	−2.45	−13.05
Erlotinib	−47.65	−146.57	167.75	−4.32	−30.79
EGFR-backbone	−33.10	−14.21	29.35	−3.60	−21.57

From Table 3, it is evident that the binding free energies of TCMIO90156 were lower than those of the control compound Erlotinib. The binding free energies of TCMIO90156, TCMIO98874, TCMIO5312, and TCMIO89212 were all lower compared with the binding free energy of EGFR-backbone. This suggests that these compounds may have positive effects on EGFR. Notably, the lowest binding energy observed for TCMIO90156 (-35.74 kcal/mol) was nearly three times higher than that of HMDB0037450 (-13.05 kcal/mol). This significant disparity in binding free energies might align with the substantial distinction in electrostatic energies between these two compounds. The results showed that TCMIO90156, TCMIO98874, TCMIO5312, and TCMIO89212, especially TCMIO90156, could potentially exhibit a potent inhibitory effect on EGFR.

According to the binding free energies of the complexes with AKT (Table 4), the binding free energy of the inhibitor A-443654 (-38.37 kcal/mol) was higher compared with those of TCMIO98874 (-56.32 kcal/mol), TCMIO89212 (-33.18 kcal/mol), and TCMIO90156 (-29.83 kcal/mol). Based on the estimated binding free energies, TCMIO98874 appeared to have a higher binding affinity for AKT compared with A-443654. Additionally, the binding free energy of HMDB0012243 was observed to be -21.68 kcal/mol, which is comparatively lower than those of the other HMDB compounds listed in Table 4. Consequently, TCMIO98874, TCMIO89212, and TCMIO90156 have been identified as potential dual inhibitors of EGFR and AKT, based on the aforementioned findings.

Table 4. MM-PBSA binding free energies and energy components (kcal/mol) of the complexes of AKT and screened TCMIO and HMDB compounds.

Ligands	$\Delta E_{\text{vander Waal}}$	$\Delta E_{\text{electrostatic}}$	$\Delta E_{\text{polar Solvation}}$	SASA	$\Delta G_{\text{binding}}$
TCMIO98874	-52.28	-647.65	648.81	-5.20	-56.32
TCMIO89212	-52.31	-262.09	285.63	-4.41	-33.18
TCMIO90156	-31.11	-310.42	312.20	-3.50	-29.83
TCMIO5312	-29.42	-261.69	275.08	-3.88	-19.91
HMDB0012243	-35.02	-61.14	78.35	-3.87	-21.68
HMDB0014570	-42.16	-29.37	54.73	-3.88	-20.68
HMDB0037450	-36.89	-74.53	111.81	-4.39	-4.00
A-443654	-42.52	-270.18	278.73	-4.4	-38.37
AKT-backbone	-42.98	-274.20	276.02	-4.43	-45.59

2.2.4. Analysis of the Interaction between Ligands and Proteins

Interaction energy decomposition analyses were performed for the protein–ligand complexes involving TCMIO89212, TCMIO90156, and TCMIO98874 with both EGFR and AKT. The results of these analyses can be observed in (Figures 12 and 13). Figure 12 demonstrates that Erlotinib exhibited robust interactions with the residues Val32 and Leu150 of EGFR. On the other hand, in the case of TCMIO89212, TCMIO90156, and TCMIO98874, the binding energies primarily relied on the contributions from different residue pairs: Val32 and Leu150; Asn148 and Leu150; and Asp161 and Val32, respectively. These findings shed light on the key residues involved in the binding interactions between these ligands and EGFR.

Figures 14 and 15 illustrate the energy contributions of the crucial EGFR and AKT residues throughout the MD simulation precesses involving TCMIO89212, TCMIO90156, and TCMIO98874. The MD simulations showed that key residues in the Erlotinib–EGFR complex, Val32 and Leu150 with TCMIO89212, Asn148 and Leu150 with TCMIO90156, and Asp161 and Val32 with TCMIO98874 maintained crucial interactions throughout the MD simulation processes. This suggests that these residues are important for the molecular recognition and binding of these ligands with EGFR. During the MD simulations of AKT, it was observed that the key residue interactions of Asp148, Asn135, and Glu85 with the positive drug A-443654, Glu91 with TCMIO89212, Glu91 with TCMIO90156, and Glu134 and Glu91 with TCMIO98874 were consistently maintained.

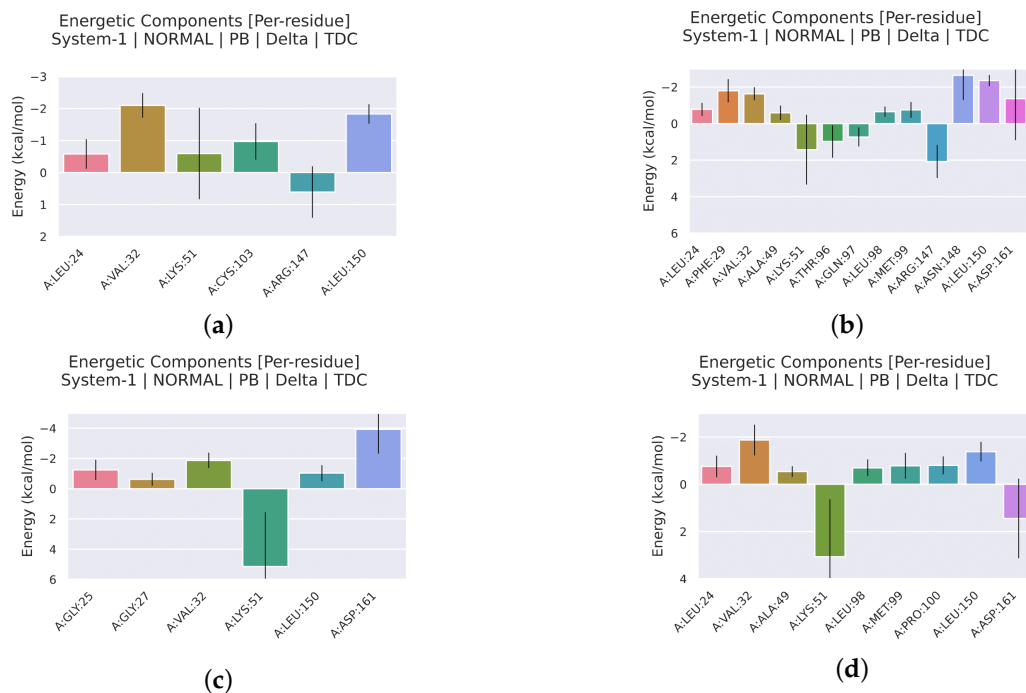


Figure 12. MMPBSA energy residue decomposition analysis of (a) TCMIO89212, (b) TCMIO90156, (c) TCMIO98874, and (d) Erlotinib with EGFR.

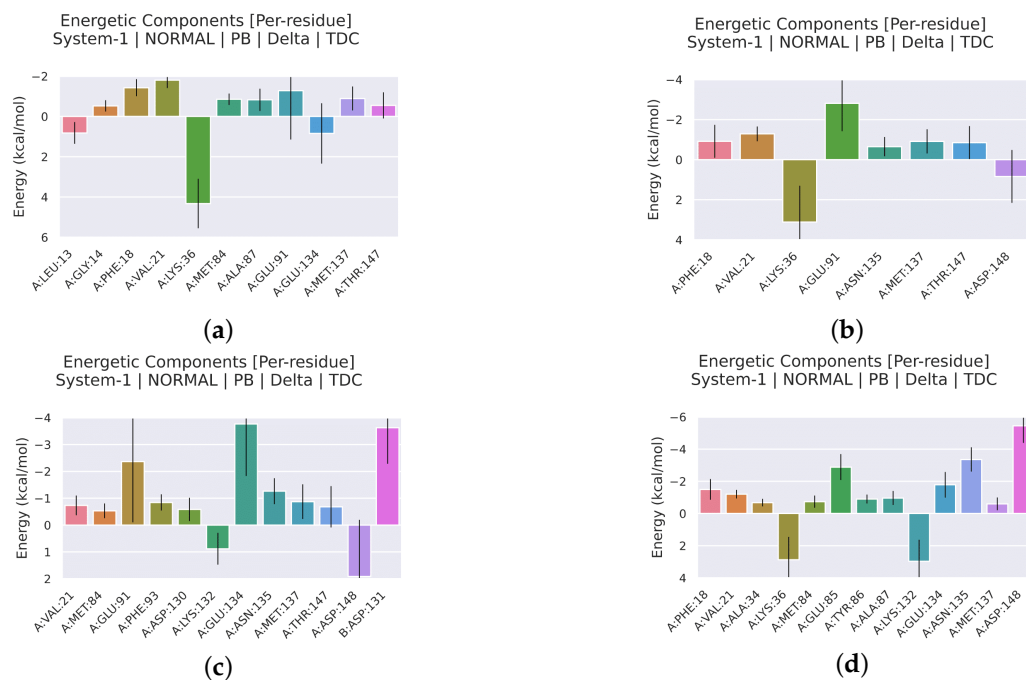


Figure 13. MMPBSA energy residue decomposition analysis of (a) TCMIO89212, (b) TCMIO90156, (c) TCMIO98874, and (d) A-443654 with AKT.

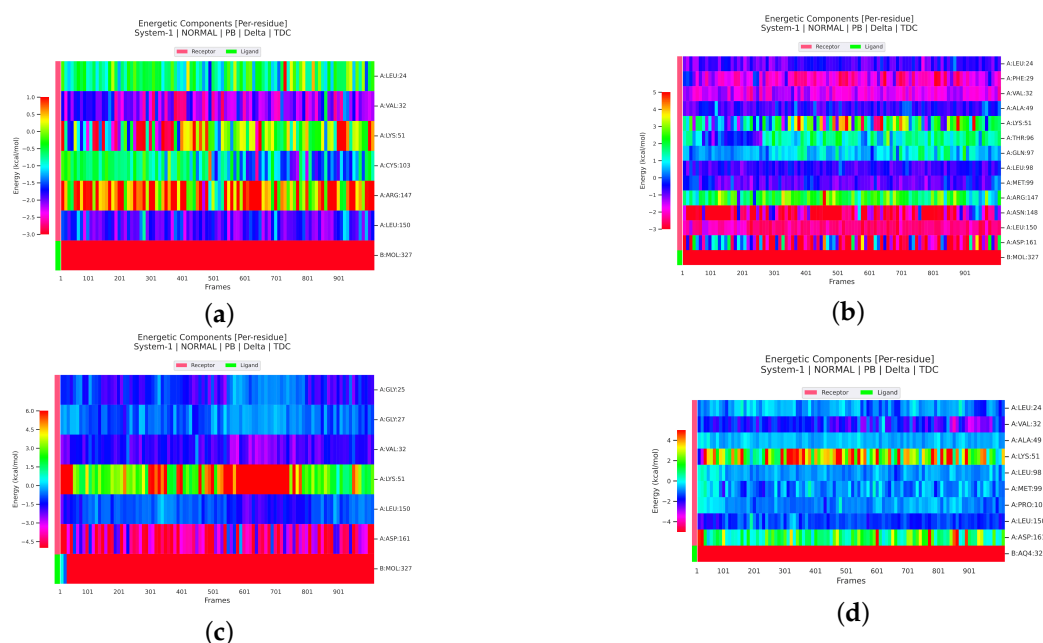


Figure 14. Analysis of MMPBSA energy residue decomposition heatmaps of (a) TCMIO89212, (b) TCMIO90156, (c) TCMIO98874, and (d) Erlotinib with EGFR. Different colors represent different energy values, and the more negative energy values in each row, the stronger the interaction between the corresponding residues of that row and small molecules.

Figure 15 reveals that the positive drug A-443654 exhibited stronger interactions with Asp148, Asn135, and Glu85 of AKT. As for TCMIO89212, TCMIO90156, and TCMIO98874, the residues Val21, Phe18, and Glu91; Glu91; and Glu134 and Glu91, respectively, significantly contributed to the binding energies.

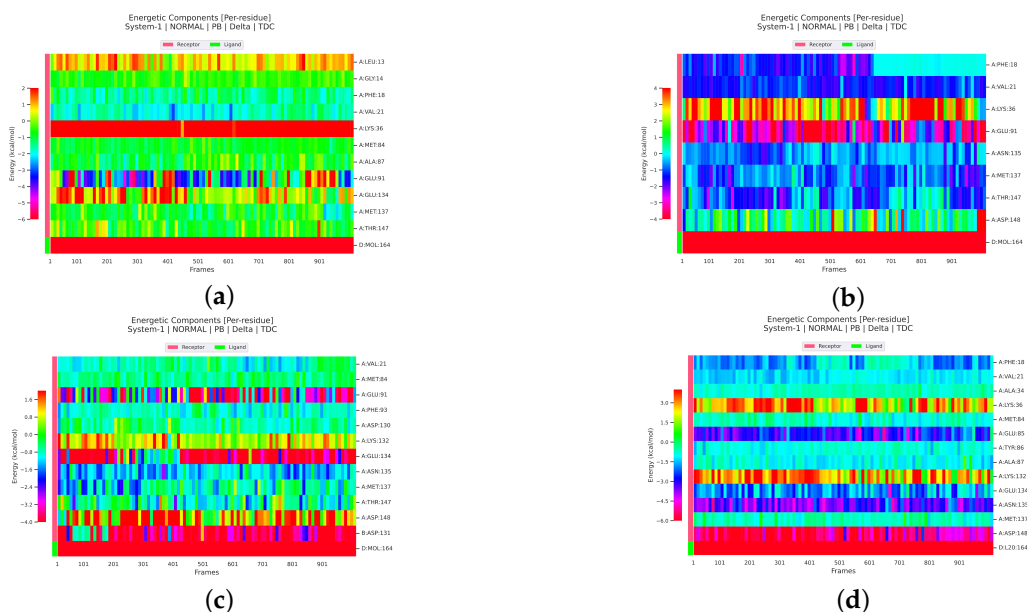


Figure 15. Analysis of MMPBSA energy residue decomposition heatmaps of (a) TCMIO89212, (b) TCMIO90156, (c) TCMIO98874, and (d) A-443654 with AKT. Different colors represent different energy values, and the more negative energy values in each row, the stronger the interaction between the corresponding residues of that row and small molecules.

2.2.5. ADMET Profiling

ADMET analyses were conducted for TCMIO90156, TCMIO89212, and TCMIO98874. The pink region depicted in Figure 16 represents the optimal range for each characteristic, with lipophiles (XLOGP3) spanning from -0.7 to $+5.0$. The size varied from 150 to 500 g/mol, the polar TPSA spanned from 20 to 130 Å², the solubility (LogS) ranged from -6 to 0, and the unsaturation fraction ranged from 0.25 to 1. The ADMET prediction results (Figure 16) indicated that all three compounds satisfied the restriction criteria of ADMET, suggesting a lower potential for toxicity risk.

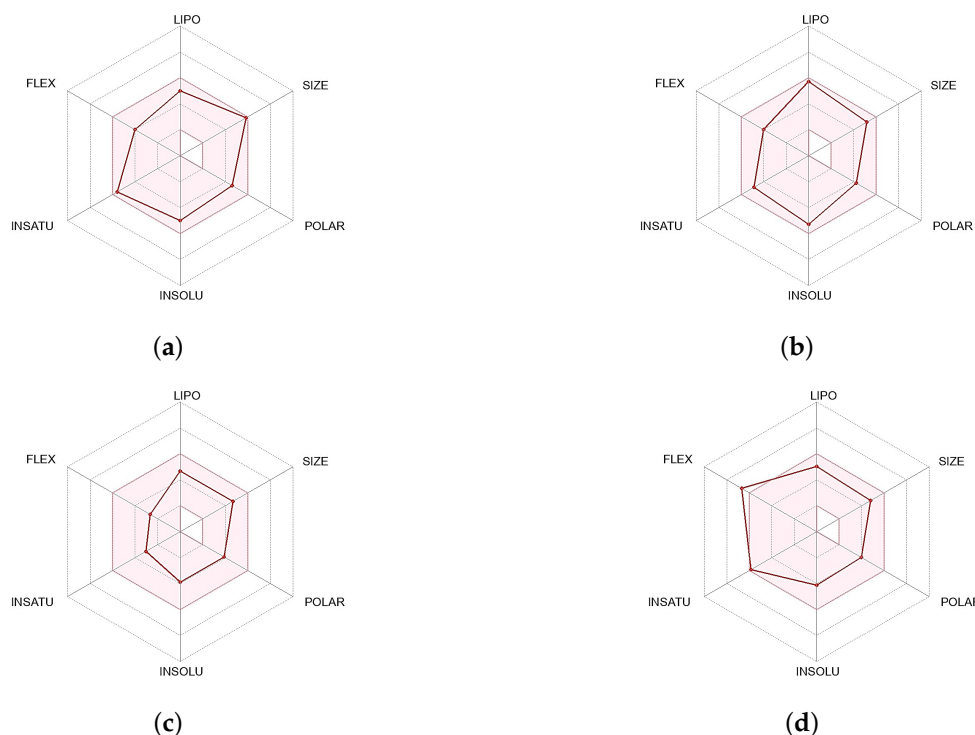


Figure 16. ADMET analyses of (a) TCMIO90156, (b) TCMIO89212, (c) TCMIO98874, and (d) Erlotinib. The color area is the suitable physicochemical space for oral bioavailability. The line represent the various parameter values predicted by the platform for compounds.

3. Screening Methods

3.1. Pharmacophore and Molecular Docking

MOE 2022 was used to construct a pharmacophore model with an active coverage of 0.9, query spacing of 0.6, query cluster of 1.25, feature number of 5, and default values for the remaining parameters. For the generation of pharmacophore models, a training set consisting of 20 known EGFR inhibitors with diverse structures was obtained from the BindingDB database [44], and the IC₅₀ values of these inhibitors ranged between 0.13 nmol/L and 1000 nmol/L. Finally, a pharmacophore model containing three characteristics, aromatics (AROs), an H-bond donor (Don2), and hydrophobicity (Hyd), was constructed (Figure 1). Virtual screenings using the pharmacophore model were performed to search for inhibitor candidates in the TCMIO database (126,973 compounds) and HMDB database (113,983 compounds). The pharmacophore model successfully filtered out a total of 3252 compounds.

Subsequently, molecular docking screenings were conducted using MOE 2022 with the application of an Amber10: ETH force field. During the molecular docking process, the receptor was set as rigid, and for each compound docking, a total of 5 optimal compound conformations were generated; the GBVI/WSA dG method [45] was used to score compound postures. The structures of EGFR (PDB 1M17) and AKT (PDB 2JDR) were employed

in this study, and were prepared by retaining the protein conformations, simultaneously using Homology Builder in MOE 2022 to complete missing protein residues and adding hydrogens. Following the pharmacophore screening, the 3252 compounds obtained were sorted based on the RMSD values, and 650 compounds of top 20% were chosen for molecular docking at the ligand-binding site of EGFR. In order to verify the docking method's effectiveness, both the test set and decoy set were subjected to the pharmacophore screening and docking with EGFR. A receiver operating characteristic ROC curve analysis was employed to assess the docking screening's capability to distinguish active compounds. Models with an area under the curve AUC value ≥ 0.7 or greater were considered to be possibly reliable [46].

The test set comprised 32 active compounds specifically targeting EGFR. This set included 20 carefully chosen inhibitors sourced from the BindingDB database. Its purpose was to assess the predictive ability of molecular docking. Additionally, a decoy set consisting of 218 inactive compounds was generated using Dude (<http://dude.docking.org/> (accessed on 16 December 2022)) in order to evaluate the efficacy of the molecular docking [47]. The decoy set was carefully assembled to consist of the compounds that share similar physical and chemical properties with the active set but no pharmacological activity [48,49]. The primary objectives was to develop a pharmacophore model which will be able to detect compounds within an active/test set, while effectively minimizing the inclusion of decoy compounds. The validation process of molecular docking screening involved the utilization of both the test and decoy sets. This validation was conducted by calculating the cumulative area under the curve (AUC) of the receiver operating characteristic (ROC) using various statistical indicators. The compounds exhibiting superior docking scores, which were lower than those of the inhibitors, were carefully chosen. Furthermore, the compounds selected based on the pharmacophore model and molecular docking of EGFR were subjected to further docking analysis within the AKT ligand-binding site. In this analysis, an AKT inhibitor was used as a reference.

3.2. Molecular Dynamics (MD) Simulations

All MD simulations were conducted employing Amber22 [50], an ff19SB force field was utilized for protein parameterization [51], and a GAFF2 force field was applied to handle compound interactions [52]. All MD simulations were run with a TIP3P water model [53,54]. The solvation simulation of receptor–ligand complex was conducted under the periodic boundary condition using a dodecahedron periodic box. The TIP3P water model was employed for solvation. To maintain charge balance in the system, Na^+ and Cl^- ions were added. Subsequently, the equilibrium phase, production simulation, and MMPBSA calculations were performed using the AmberMDrun command [55]. The ten-step simulation preparation scheme is a widely-accepted equilibrium method for solvated biomolecules. It is applicable to various types of systems and allows for simple tests based on system density to ensure simulation stability. This simulation approach has been extensively validated and has shown to be effective and versatile, having been successfully applied to diverse protein and nucleic acid systems [56]. Constant temperature was controlled with a velocity rescaling thermostat [57], and constant pressure was controlled with a Berendsen barostat [58]. The system was initially equilibrated at 300 K through 100 ps NVT and NPT simulations, respectively, and the reference pressure for the NPT ensemble was set to 1 bar.

The 100 ns MD simulations with a time step of 2 fs were performed for the complexes of the selected compounds with EGFR and AKT added. The `gmx_MMPBSA` tool was utilized to estimate the binding energy of each complex by analyzing the MD trajectory [59]. This tool calculates the binding energy based on a total of 100 frames extracted from the 100 ns production simulation trajectory.

3.3. ADMET Evaluation

The structures of the compounds were converted into the simplified molecular input line input system (SMILES) format. Subsequently, the documents were submitted to <http://www.swissadme.ch/> (accessed on 7 March 2023) SwissADME [60] to evaluate the metabolism, excretion, distribution, toxicity, and absorption characteristics of small molecules.

4. Conclusions

We employed a ligand-based pharmacophore filtration and molecular docking screening approach to identify potential natural compound inhibitors within the TCMIO database, as well as endogenous compounds in the HMDB. These compounds were targeted to simultaneously inhibit both EGFR and AKT. A total of seven compounds were discovered, demonstrating a strong alignment with the pharmacophore model and exhibiting favorable docking scores. Among them, TCMIO90156 demonstrated the lowest binding free energy when compared with the control compound Erlotinib for EGFR. Additionally, the binding free energies of TCMIO98874, TCMIO5312, and TCMIO89212 were in close proximity to the binding free energy of Erlotinib. The results obtained from the MD simulation indicated that the binding free energy of TCMIO98874 with AKT was lower compared with the control compound A-443654. On the other hand, the binding free energies of TCMIO90156 and TCMIO89212 were slightly higher than that of A-443654. The analysis of their interactions with EGFR showed that these compounds exhibited similar interaction patterns with the reference drugs of EGFR. Furthermore, MD simulations indicated that TCMIO90156, TCMIO89212, and TCMIO98874 displayed relatively low binding free energies and formed crucial bindings with the essential residues of both EGFR and AKT. These findings suggest that these compounds have the potential to function as dual-target inhibitors, simultaneously targeting both EGFR and AKT. The findings of this study offer valuable insights for further experimental investigations. The goal moving forward is to develop a web-based platform that provides a user-friendly dataset of EGFR inhibitors, as described in article [61]. This will serve as a valuable resource for researchers in the field.

Supplementary Materials: The following supporting information can be downloaded at: <https://www.mdpi.com/article/10.3390/molecules28227607/s1>, Figure S1: ADMET analyze of TCMIO5312, HMDB0012243, HMDB0014570, HMDB0037450; Figure S2: RMSF of AKT complexes; Figure S3: Rg of AKT complexes; Figure S4: H-bond analyses of EGFR complexes (a) TCMIO5312, (b) HMDB0012243, (c) HMDB0037450, (d) HMDB0014570; Figure S5: H-bond analyses of AKT complexes H-bond analyses of AKT complexes (a) TCMIO5312, (b) TCMIO89212, (c) TCMIO90156, (d) TCMIO98874, (e) HMDB0012243, (f) HMDB0037450, (g) HMDB0014570, (h) A-443654; Table S1. The full list of the active ligands used.

Author Contributions: H.Y., formal analysis, resources, data curation, writing, and original draft preparation; Z.Z., methodology and software; Q.L., investigation; C.L., validation; J.Y., formal analysis; W.L., management and writing. All authors have read and agreed to the published version of the manuscript.

Funding: This work was supported by the Natural Science Foundation of Shandong Province of China (ZR2020QB104).

Institutional Review Board Statement: Not applicable.

Informed Consent Statement: Not applicable.

Data Availability Statement: Data are contained within the article and Supplementary Materials.

Conflicts of Interest: The authors declare no conflict of interest.

Abbreviations

The following abbreviations are used in this manuscript:

ΔE_{SASA} Solvent accessible surface area

References

1. Seshacharyulu, P.; Ponnusamy, M.P.; Haridas, D.; Jain, M.; Ganti, A.K.; Batra, S.K. Targeting the EGFR signaling pathway in cancer therapy. *Expert Opin. Ther. Targets* **2012**, *16*, 15–31. [[CrossRef](#)]
2. Harari, P.M. Epidermal growth factor receptor inhibition strategies in oncology. *Endocr.-Relat. Cancer Endocr Relat Cancer* **2004**, *11*, 689–708. [[CrossRef](#)]
3. Yewale, C.; Baradia, D.; Vhora, I.; Patil, S.; Misra, A. Epidermal growth factor receptor targeting in cancer: A review of trends and strategies. *Biomaterials* **2013**, *34*, 8690–8707. [[CrossRef](#)]
4. Wu, W.W.; Ye, Z.J.; Xu, Y.M.; Zhang, J.; Tang, J.S. Ergosta-7, 22-diene-2 β , 3 α , 9 α -triol (EGDT) from *Ganoderma lucidum* inhibits nasopharyngeal carcinoma cells by blocking EGFR signaling pathway. *Chin. Herb. Med.* **2018**, *10*, 27–33. [[CrossRef](#)]
5. Yang, T.; Guo, Q.; Shi, X.; Wu, S.; Li, Y.; Sun, Y.; Zhao, Y.; Chai, L.; Gao, Y.; Lou, L.; et al. Panax notoginseng saponins promotes cerebral recovery from ischemic injury by downregulating LINGO-1 and activating the EGFR/PI3K/AKT signaling pathways in vivo. *J. Tradit. Chin. Med. Sci.* **2018**, *5*, 151–160. [[CrossRef](#)]
6. Westover, D.; Zugazagoitia, J.; Cho, B.; Lovly, C.; Paz-Ares, L. Mechanisms of acquired resistance to first- and second-generation EGFR tyrosine kinase inhibitors. *Ann. Oncol.* **2018**, *29*, i10–i19. [[CrossRef](#)]
7. Passaro, A.; Mok, T.; Peters, S.; Popat, S.; Ahn, M.J.; De Marinis, F. Recent advances on the role of EGFR tyrosine kinase inhibitors in the management of NSCLC with uncommon, non exon 20 insertions, EGFR mutations. *J. Thorac. Oncol.* **2021**, *16*, 764–773. [[CrossRef](#)]
8. Sequist, L.V.; Han, J.Y.; Ahn, M.J.; Cho, B.C.; Yu, H.; Kim, S.W.; Yang, J.C.H.; Lee, J.S.; Su, W.C.; Kowalski, D.; et al. Osimertinib plus savolitinib in patients with EGFR mutation-positive, MET-amplified, non-small-cell lung cancer after progression on EGFR tyrosine kinase inhibitors: Interim results from a multicentre, open-label, phase 1b study. *Lancet Oncol.* **2020**, *21*, 373–386. [[CrossRef](#)]
9. Wu, Y.L.; Cheng, Y.; Zhou, J.; Lu, S.; Zhang, Y.; Zhao, J.; Kim, D.W.; Soo, R.A.; Kim, S.W.; Pan, H.; et al. Tepotinib plus gefitinib in patients with EGFR-mutant non-small-cell lung cancer with MET overexpression or MET amplification and acquired resistance to previous EGFR inhibitor (INSIGHT study): An open-label, phase 1b/2, multicentre, randomised trial. *Lancet Respir. Med.* **2020**, *8*, 1132–1143. [[CrossRef](#)]
10. El Guerrab, A.; Bamdad, M.; Bignon, Y.J.; Penault-Llorca, F.; Aubeil, C. Co-targeting EGFR and mTOR with gefitinib and everolimus in triple-negative breast cancer cells. *Sci. Rep.* **2020**, *10*, 6367. [[CrossRef](#)]
11. Park, S.Y.; Kim, Y.M.; Pyo, H. Gefitinib radiosensitizes non-small cell lung cancer cells through inhibition of ataxia telangiectasia mutated. *Mol. Cancer* **2010**, *9*, 222. [[CrossRef](#)]
12. Anderson, N.G.; Ahmad, T.; Chan, K.; Dobson, R.; Bundred, N.J. ZD1839 (Iressa), a novel epidermal growth factor receptor (EGFR) tyrosine kinase inhibitor, potently inhibits the growth of EGFR-positive cancer cell lines with or without erbB2 overexpression. *Int. J. Cancer* **2001**, *94*, 774–782. [[CrossRef](#)]
13. Bencardino, K.; Manzoni, M.; Delfanti, S.; Riccardi, A.; Danova, M.; Corazza, G. Epidermal growth factor receptor tyrosine kinase inhibitors for the treatment of non-small-cell lung cancer: Results and open issues. *Intern. Emerg. Med.* **2007**, *2*, 3–12. [[CrossRef](#)]
14. Hochmair, M.J.; Buder, A.; Schwab, S.; Burghuber, O.C.; Prosch, H.; Hilbe, W.; Cseh, A.; Fritz, R.; Filipits, M. Liquid-biopsy-based identification of EGFR T790M mutation-mediated resistance to afatinib treatment in patients with advanced EGFR mutation-positive NSCLC, and subsequent response to osimertinib. *Target. Oncol.* **2019**, *14*, 75–83. [[CrossRef](#)]
15. Lin, N.U.; Winer, E.P.; Wheatley, D.; Carey, L.A.; Houston, S.; Mendelson, D.; Munster, P.; Frakes, L.; Kelly, S.; Garcia, A.A.; et al. A phase II study of afatinib (BIBW 2992), an irreversible ErbB family blocker, in patients with HER2-positive metastatic breast cancer progressing after trastuzumab. *Breast Cancer Res. Treat.* **2012**, *133*, 1057–1065. [[CrossRef](#)] [[PubMed](#)]
16. Lazzari, C.; Gregorc, V.; Karachaliou, N.; Rosell, R.; Santarpia, M. Mechanisms of resistance to osimertinib. *J. Thorac. Dis.* **2020**, *12*, 2851. [[CrossRef](#)] [[PubMed](#)]
17. Mok, T.S.; Wu, Y.L.; Ahn, M.J.; Garassino, M.C.; Kim, H.R.; Ramalingam, S.S.; Shepherd, F.A.; He, Y.; Akamatsu, H.; Theelen, W.S.; et al. Osimertinib or Platinum-Pemetrexed in EGFR T790M-Positive Lung Cancer. *N. Engl. J. Med.* **2017**, *376*, 629–640. [[CrossRef](#)]
18. Yin, B.; Fang, D.M.; Zhou, X.L.; Gao, F. Natural products as important tyrosine kinase inhibitors. *Eur. J. Med. Chem.* **2019**, *182*, 111664. [[CrossRef](#)]
19. Abou-Zied, H.A.; Youssif, B.; Mohamed, M.; Hayallah, A.M.; Abdel-Aziz, M. EGFR inhibitors and apoptotic inducers: Design, synthesis, anticancer activity and docking studies of novel xanthine derivatives carrying chalcone moiety as hybrid molecules. *Bioorg. Chem.* **2019**, *89*, 102997. [[CrossRef](#)] [[PubMed](#)]
20. Abdelgawad, M.A.; Musa, A.; Almalki, A.H.; Alzarea, S.I.; Mostafa, E.M.; Hegazy, M.M.; Mostafa-Hedeab, G.; Ghoneim, M.M.; Parambi, D.G.; Bakr, R.B.; et al. Novel phenolic compounds as potential dual EGFR and COX-2 inhibitors: Design, semisynthesis, in vitro biological evaluation and in silico insights. *Drug Des. Dev. Ther.* **2021**, *15*, 2325–2337. [[CrossRef](#)]
21. Acevedo.; Chonny.; Herrera.; Scotti.; Luciana.; Marcus.; Tullius. In Silico Studies Designed to Select Sesquiterpene Lactones with Potential Antichagasic Activity from an In-House Asteraceae Database. *ChemMedChem* **2018**, *13*, 634–645. [[CrossRef](#)]
22. Wheeler, D.; Dunn, E.; Harari, P. Understanding resistance to EGFR inhibitors-impact on future treatment strategies. *Nat. Rev. Clin. Oncol.* **2010**, *7*, 493–507. [[CrossRef](#)]
23. Brognard, J.; Clark, A.S.; Ni, Y.; Dennis, P.A. Akt/Protein Kinase B Is Constitutively Active in Non-Small Cell Lung Cancer Cells and Promotes Cellular Survival and Resistance to Chemotherapy and Radiation. *Cancer Res.* **2001**, *61*, 3986.

24. Pan, Q.; Lu, Y.; Xie, L.; Wu, D.; Liu, R.; Gao, W.; Luo, K.; He, B.; Pu, Y. Recent Advances in Boosting EGFR Tyrosine Kinase Inhibitors-Based Cancer Therapy. *Mol. Pharm.* **2023**, *20*, 829–852. [[CrossRef](#)] [[PubMed](#)]
25. Hu, L.; Fan, M.; Shi, S.; Song, X.; Wang, F.; He, H.; Qi, B. Dual target inhibitors based on EGFR: Promising anticancer agents for the treatment of cancers (2017-). *Eur. J. Med. Chem.* **2022**, *227*, 113963. [[CrossRef](#)] [[PubMed](#)]
26. Choowongkamon, K.; Sawatdichaikul, O.; Songtawee, N.; Limtrakul, J. Receptor-Based Virtual Screening of EGFR Kinase Inhibitors from the NCI Diversity Database. *Molecules* **2010**, *15*, 4041–4054. [[CrossRef](#)]
27. Chuang, C.H.; Cheng, T.C.; Leu, Y.L.; Chuang, K.H.; Tzou, S.C.; Chen, C.S. Discovery of Akt Kinase Inhibitors through Structure-Based Virtual Screening and Their Evaluation as Potential Anticancer Agents. *Int. J. Mol. Sci.* **2015**, *16*, 3202–3212. [[CrossRef](#)]
28. Lopez-Vallejo, F.; Caulfield, T.; Martinez-Mayorga, K.; A. Giulianotti, M.; Nefzi, A.; A. Houghten, R.; L. Medina-Franco, J. Integrating Virtual Screening and Combinatorial Chemistry for Accelerated Drug Discovery. *Comb. Chem. High Throughput Screen.* **2011**, *14*, 475–487. [[CrossRef](#)] [[PubMed](#)]
29. Bono, A.; Lauria, A.; La Monica, G.; Alamia, F.; Mingoia, F.; Martorana, A. In Silico Design of New Dual Inhibitors of SARS-CoV-2 MPRO through Ligand- and Structure-Based Methods. *Int. J. Mol. Sci.* **2023**, *24*, 8377. [[CrossRef](#)]
30. López-López, E.; Prieto-Martínez, F.D.; Medina-Franco, J.L. Activity landscape and molecular modeling to explore the SAR of dual epigenetic inhibitors: A focus on G9a and DNMT1. *Molecules* **2018**, *23*, 3282. [[CrossRef](#)]
31. Tarozzi, A.; Marchetti, C.; Nicolini, B.; D'Amico, M.; Ticchi, N.; Pruccoli, L.; Tumiatti, V.; Simoni, E.; Lodola, A.; Mor, M.; et al. Combined inhibition of the EGFR/AKT pathways by a novel conjugate of quinazoline with isothiocyanate. *Eur. J. Med. Chem.* **2016**, *117*, 283–291. [[CrossRef](#)] [[PubMed](#)]
32. Liu, Z.; Cai, C.; Du, J.; Liu, B.; Cui, L.; Fan, X.; Wu, Q.; Fang, J.; Xie, L. TCMIO: A comprehensive database of traditional Chinese medicine on immuno-oncology. *Front. Pharmacol.* **2020**, *11*, 439. [[CrossRef](#)] [[PubMed](#)]
33. Wishart, D.S.; Tzur, D.; Knox, C.; Eisner, R.; Guo, A.C.; Young, N.; Cheng, D.; Jewell, K.; Arndt, D.; Sawhney, S.; et al. HMDB: The human metabolome database. *Nucleic Acids Res.* **2007**, *35*, D521–D526. [[CrossRef](#)] [[PubMed](#)]
34. Wissner, A.; Fraser, H.L.; Ingalls, C.L.; Dushin, R.G.; Floyd, M.B.; Cheung, K.; Nittoli, T.; Ravi, M.R.; Tan, X.; Loganzo, F. Dual irreversible kinase inhibitors: Quinazoline-based inhibitors incorporating two independent reactive centers with each targeting different cysteine residues in the kinase domains of EGFR and VEGFR-2. *Bioorg. Med. Chem.* **2007**, *15*, 3635–3648. [[CrossRef](#)]
35. Yang, Y.A.; Tang, W.J.; Zhang, X.; Yuan, J.W.; Liu, X.H.; Zhu, H.L. Synthesis, molecular docking and biological evaluation of glycyrrhizin analogs as anticancer agents targeting EGFR. *Molecules* **2014**, *19*, 6368–6381. [[CrossRef](#)]
36. Peng, Y.H.; Shiao, H.Y.; Tu, C.H.; Liu, P.M.; Hsu, J.T.A.; Amancha, P.K.; Wu, J.S.; Coumar, M.S.; Chen, C.H.; Wang, S.Y.; et al. Protein Kinase Inhibitor Design by Targeting the Asp-Phe-Gly (DFG) Motif: The Role of the DFG Motif in the Design of Epidermal Growth Factor Receptor Inhibitors. *J. Med. Chem.* **2013**, *56*, 3889–3903. [[CrossRef](#)]
37. Zarezade, V.; Abolghasemi, M.; Rahim, F.; Veisi, A.; Behbahani, M. In silico assessment of new progesterone receptor inhibitors using molecular dynamics: A new insight into breast cancer treatment. *J. Mol. Model.* **2018**, *24*, 337. [[CrossRef](#)]
38. Zarezade, V.; Rezaei, H.; Shakerinezhad, G.; Safavi, A.; Nazeri, Z.; Veisi, A.; Azadbakht, O.; Hatami, M.; Sabaghan, M.; Shajirat, Z. The identification of novel inhibitors of human angiotensin-converting enzyme 2 and main protease of Sars-Cov-2: A combination of in silico methods for treatment of COVID-19. *J. Mol. Struct.* **2021**, *1237*, 130409. [[CrossRef](#)]
39. Lobanov, M.Y.; Bogatyreva, N.; Galzitskaya, O. Radius of gyration as an indicator of protein structure compactness. *Mol. Biol.* **2008**, *42*, 623–628. [[CrossRef](#)]
40. Méndez-Luna, D.; Martínez-Archundia, M.; Maroun, R.C.; Ceballos-Reyes, G.; Fragoso-Vázquez, M.; González-Juárez, D.; Correa-Basurto, J. Deciphering the GPER/GPR30-agonist and antagonists interactions using molecular modeling studies, molecular dynamics, and docking simulations. *J. Biomol. Struct. Dyn.* **2015**, *33*, 2161–2172. [[CrossRef](#)]
41. Aghahari, A.K.; Sneha, P.; Doss, C.G.P.; Siva, R.; Zayed, H. A profound computational study to prioritize the disease-causing mutations in PRPS1 gene. *Metab. Brain Dis.* **2017**, *33*, 589–600. [[CrossRef](#)] [[PubMed](#)]
42. Priya, R.; Sumitha, R.; Doss, C.; Rajasekaran, C.; Siva, R. Molecular Docking and Molecular Dynamics to Identify a Novel Human Immunodeficiency Virus Inhibitor from Alkaloids of *Toddalia asiatica*. *Pharmacogn. Mag.* **2015**, *11*, S414. [[PubMed](#)]
43. Poli, G.; Granchi, C.; Rizzolio, F.; Tuccinardi, T. Application of MM-PBSA methods in virtual screening. *Molecules* **2020**, *25*, 1971. [[CrossRef](#)] [[PubMed](#)]
44. Liu, T.; Lin, Y.; Wen, X.; Jorissen, R.N.; Gilson, M.K. BindingDB: A web-accessible database of experimentally determined protein–ligand binding affinities. *Nucleic Acids Res.* **2007**, *35*, D198–D201. [[CrossRef](#)]
45. Corbeil, C.R.; Williams, C.I.; Labute, P. Variability in docking success rates due to dataset preparation. *J.-Comput.-Aided Mol. Des.* **2012**, *26*, 775–786. [[CrossRef](#)]
46. Empeur-Mot, C.; Zagury, J.F.; Montes, M. Screening Explorer—An Interactive Tool for the Analysis of Screening Results. *J. Chem. Inf. Model.* **2016**, *56*, 2281–2286. [[CrossRef](#)]
47. Mysinger, M.M.; Carchia, M.; Irwin, J.J.; Shoichet, B.K. Directory of useful decoys, enhanced (DUD-E): Better ligands and decoys for better benchmarking. *J. Med. Chem.* **2012**, *55*, 6582–6594. [[CrossRef](#)]
48. Lipinski, C.A. Lead- and drug-like compounds: The rule-of-five revolution. *Drug Discov. Today Technol.* **2004**, *1*, 337–341. [[CrossRef](#)]
49. Yadav, A.V.; Shete, A.S.; Dabke, A.P.; Kulkarni, P.V.; Sakhare, S.S. Co-Crystals: A Novel Approach to Modify Physicochemical Properties of Active Pharmaceutical Ingredients. *Indian J. Pharm. Sci.* **2009**, *71*, 359–370. [[CrossRef](#)]

50. Case, D.; Aktulga, H.; Belfon, K.; Ben-Shalom, I.; Berryman, J.; Brozell, S.; Cerutti, D.; Cheatham, T., III.; Cisneros, G.; *In Proceedings of the Amber 2022*; University of California: San Francisco, CA, USA, 2022.
51. Tian, C.; Kasavajhala, K.; Belfon, K.A.A.; Raguette, L.; Huang, H.; Migués, A.N.; Bickel, J.; Wang, Y.; Pincay, J.; Wu, Q.; et al. ff19SB: Amino-Acid-Specific Protein Backbone Parameters Trained against Quantum Mechanics Energy Surfaces in Solution. *J. Chem. Theory Comput.* **2020**, *16*, 528–552. [[CrossRef](#)]
52. Vassetti, D.; Pagliai, M.; Procacci, P. Assessment of GAFF2 and OPLS-AA General Force Fields in Combination with the Water Models TIP3P, SPCE, and OPC3 for the Solvation Free Energy of Druglike Organic Molecules. *J. Chem. Theory Comput.* **2019**, *15*, 1983–1995. [[CrossRef](#)] [[PubMed](#)]
53. Mark, P.; Nilsson, L. Structure and Dynamics of the TIP3P, SPC, and SPC/E Water Models at 298 K. *J. Phys. Chem.* **2001**, *105*, 9954–9960. [[CrossRef](#)]
54. Price, D.J.; Brooks, C.L., III. A modified TIP3P water potential for simulation with Ewald summation. *J. Chem. Phys.* **2004**, *121*, 10096–10103. [[CrossRef](#)]
55. Zhang, Z.W.; Lu, W.C. AmberMDrun: A Scripting Tool for Running Amber MD in an Easy Way. *Biomolecules* **2023**, *13*, 635. [[CrossRef](#)]
56. Roe, D.R.; Brooks, B.R. A protocol for preparing explicitly solvated systems for stable molecular dynamics simulations. *J. Chem. Phys.* **2020**, *153*, 054123. [[CrossRef](#)]
57. Bussi, G.; Donadio, D.; Parrinello, M. Canonical sampling through velocity rescaling. *J. Chem. Phys.* **2007**, *126*, 014101. [[CrossRef](#)]
58. Andersen, H.C. Molecular dynamics simulations at constant pressure and/or temperature. *J. Chem. Phys.* **2008**, *72*, 2384–2393. [[CrossRef](#)]
59. Miller, B.R.; Mcgee, T.D.; Swails, J.M.; Homeyer, N.; Roitberg, A.E. MMPBSA.py: An efficient program for end-state free energy calculations. *J. Chem. Theory Comput.* **2012**, *8*, 3314–3321. [[CrossRef](#)]
60. Daina, A.; Michielin, O.; Zoete, V. SwissADME: A free web tool to evaluate pharmacokinetics, drug-likeness and medicinal chemistry friendliness of small molecules. *Sci. Rep.* **2017**, *7*, 42717. [[CrossRef](#)]
61. Cui, Z.; Zhang, Z.; Zhou, T.; Zhou, X.; Zhang, Y.; Meng, H.; Wang, W.; Liu, Y. A TastePeptides-Meta system including an umami/bitter classification model Umami_YYDS, a TastePeptidesDB database and an open-source package Auto_Taste_ML. *Food Chem.* **2023**, *405*, 134812. [[CrossRef](#)]

Disclaimer/Publisher’s Note: The statements, opinions and data contained in all publications are solely those of the individual author(s) and contributor(s) and not of MDPI and/or the editor(s). MDPI and/or the editor(s) disclaim responsibility for any injury to people or property resulting from any ideas, methods, instructions or products referred to in the content.